



HAL
open science

Generation of three-dimensional patterns through wave interaction in a model of free surface swirling flow

David Fabre, Jérôme Mougel

► **To cite this version:**

David Fabre, Jérôme Mougel. Generation of three-dimensional patterns through wave interaction in a model of free surface swirling flow. *Fluid Dynamics Research*, 2014, 46 (6), pp.1-20. 10.1088/0169-5983/46/6/061415 . hal-03519800

HAL Id: hal-03519800

<https://hal.science/hal-03519800v1>

Submitted on 10 Jan 2022

HAL is a multi-disciplinary open access archive for the deposit and dissemination of scientific research documents, whether they are published or not. The documents may come from teaching and research institutions in France or abroad, or from public or private research centers.

L'archive ouverte pluridisciplinaire **HAL**, est destinée au dépôt et à la diffusion de documents scientifiques de niveau recherche, publiés ou non, émanant des établissements d'enseignement et de recherche français ou étrangers, des laboratoires publics ou privés.



Open Archive TOULOUSE Archive Ouverte (OATAO)

OATAO is an open access repository that collects the work of Toulouse researchers and makes it freely available over the web where possible.

This is an author-deposited version published in : <http://oatao.univ-toulouse.fr/>
Eprints ID : 14408

To link to this article : DOI : 10.1088/0169-5983/46/6/061415
URL : <http://dx.doi.org/10.1088/0169-5983/46/6/061415>

To cite this version : Fabre, David and Mougel, Jerome [Generation of three-dimensional patterns through wave interaction in a model of free surface swirling flow](#). (2014) Fluid Dynamics Research, vol. 46 (n° 6). n/a. ISSN 0169-5983

Any correspondence concerning this service should be sent to the repository administrator: staff-oatao@listes-diff.inp-toulouse.fr

Generation of three-dimensional patterns through wave interaction in a model of free surface swirling flow

D. Fabre & J. Mougel

¹ Institut de Mécanique des Fluides de Toulouse (IMFT), University of Toulouse

Abstract.

The free surface flow in a cylindrical tank over a rotating bottom is known to support spectacular three-dimensional patterns, including deformation of the inner free surface into the shape of rotating polygons, and sloshing behavior of the upper free surface (e.g. Iga et al., FDR 2014, same issue). Through a stability analysis of a simplified model of this flow, we show that such patterns can be explained as a resonance mechanism involving different families of waves. The approach extends a previous work (Tophøj et al., PRL 2013) which explained the rotating polygons as an interaction between gravity waves and centrifugal waves, under the assumption that the base flow can be modeled as a potential vortex. We show that this previous model is justified for strong rotation rates (Dry-Potential case), and that for weaker rotations it can be improved by introducing an inner vortex core in solid-body rotation, which either extends to the center of the plate (Wet case) or surrounds a dry central region (Dry-Composite case). The study of this improved model predicts two new kind of instabilities. The first occurs at low rotations (Wet case) and results from an interaction between gravity waves and the Kelvin-Kirchhoff wave (namely, oscillation of the boundary of the vortex core). This instability is proposed to be at the origin of the sloshing phenomenon. The second new instability occurs, for moderate rotations, (Dry-Composite case) as an interaction between gravity waves and a "Kelvin-Centrifugal" wave characterized by deformation of the inner surface and the vortex core boundary in opposite directions. This instability exists for all azimuthal wave numbers starting from $m = 1$, this case corresponding to a "monogon" pattern.

Keywords: Rotating flow, free surface waves, instabilities, sloshing.

1. Introduction

Rotating flows with a free surface are known to support spectacular three-dimensional patterns. A configuration which has been particularly studied corresponds to cylindrical container driven by a rotating bottom plate. This setup leads to the occurrence of polygonal patterns which rotate with essentially unchanged form. Initially discovered by Vatistas [1], this feature was rediscovered independently by Jansson et al. [2], which provided a state diagram in terms of the rotation frequency of the bottom plate, and the mean height of fluid in the container. Generally, as the rotation rate of the plate is increased, the numbers of corners of the polygons increase from 2 to 6. In some cases, the three-dimensional patterns occur in a recurrent way, with an alternance of a highly deformed surface of elliptical cross-section and a quasi-axisymmetric flow. This phenomenon was called "switching" by Suzuki et al. [3, 4]. A related but different phenomenon called "sloshing" has been reported [1] ‡. The latter is also a recurrent phenomenon, but corresponds to an oscillation mostly affecting the outer part of the free surface. It is observed for lower rotation rates compared to the range of existence of polygons, in a range of parameters where the plate remains entirely wet. Recently, Iga et al. [5] have conducted extensive sets of experiments, considering a wider range of parameters than previous studies. They provided an extended state diagram, covering the range of existence of all these patterns. They particularly considered the sloshing phenomenon, and observed this state for both $m = 3$ (triangles) and $m = 2$ (ellipses) azimuthal wave numbers. In particular, they showed that the $m = 3$ sloshing exists in a very narrow range of rotation frequencies, which is almost independent of the height of liquid in the container.

In a recent paper, Tophøj et al. [6] (hereafter TMBF) have shown that the polygonal patterns can be explained as the result of an instability of the axisymmetric base-flow predating their occurrence. In this study, the base flow was modeled as a simple potential vortex; a hypothesis which is supported by experimental results and theoretical arguments [7]. They first used a momentum energy balance argument to relate the circulation of the potential vortex to the rotation rate of the plate. Subsequently, using both a global stability approach and a simplified 'toy-model' in which all the motion is assumed to take place in a two-dimensional domain lying along the boundaries, they showed that this potential flow is unstable to perturbations with azimuthal wavenumber $m \geq 2$, in qualitative accordance with the experiments. They finally showed that the instability can be explained as the result of a resonance between two kinds of waves, namely gravity waves affecting the external parts of the flow where the free surface is almost horizontal, and centrifugal waves affecting the inner parts of the flow where the free surface is almost vertical.

Although the modeling of the flow as a potential vortex is justified for large rotation rates corresponding to situation where the flow displays central dry region of significant

‡ In the original paper [1] "switching" and "sloshing" are reported but without clear distinction as both phenomena where called "sloshing".

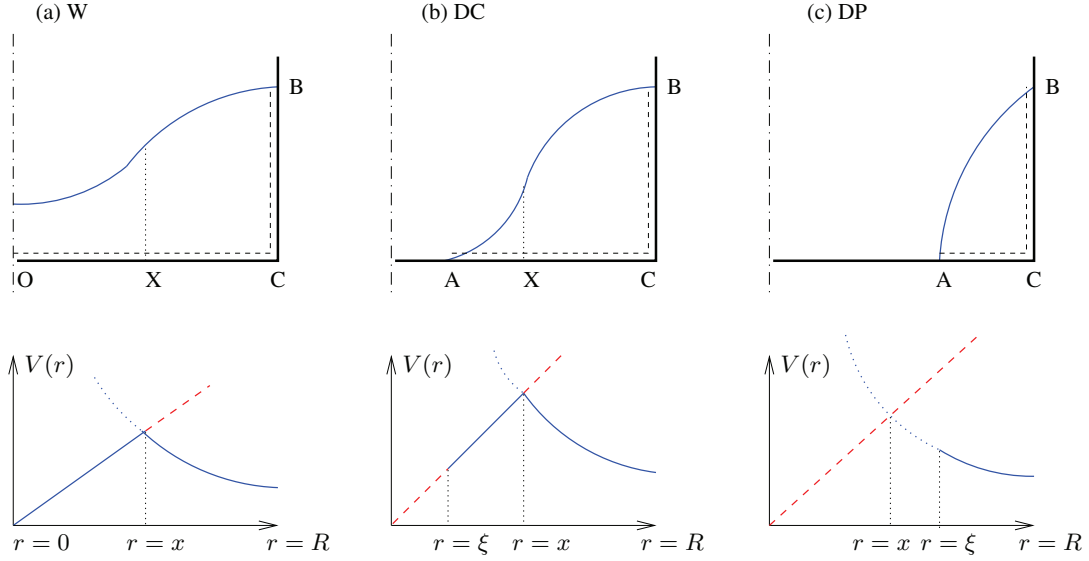


Figure 1. Description of the model in the three possible cases : (a) Wet-Composite (W), (b) Dry-Composite (DC), (c) Dry-Potential (DP). Up : Sketch of the flow featuring the shape of the free surface, and the 2D layers constituting the simplified model (bounded by the dashed lines). Bottom : angular velocity laws of the fluid (plain, blue line) and of the bottom plate (dashed, red line).

extent, experiments [7] show that it becomes insufficient at lower rotation rates. In such situation, measurement suggest that in the central parts, the velocity field is more accurately represented as a solid-body rotation. Also, the potential model is unable to explain the occurrence of the switching and sloshing phenomena, which generally exist in range of parameters where the plate remains wet.

The purpose of the present paper is thus to study an improved version of the TMBF model, in which the flow is modeled as a composite flow with a central region in solid body rotation matched to an outer region in potential rotation (thereby corresponding to the classical Rankine vortex). We first describe the model and derive its characteristics as function of the rotation rate of the plate , extending the momentum energy balance argument of TMBF (§3). We subsequently investigate the stability of this flow through a two-dimensional 'toy-model' solvable on analytic grounds, and interpret the instabilities as wave resonances (§4). We finally summarize the results (§5) and discuss their relevance with experimental observations.

2. Modelling of the base flow

2.1. The composite model

The model of axisymmetric base flow considered in this paper is sketched in figure 1. This model is parametrized by two nondimensional numbers. The first is the aspect ratio H/R where R is the radius and H and the mean height of liquid (or more properly

the height of liquid in absence of rotation). The second is the Froude number defined as

$$F = \Omega \sqrt{R/g}, \quad (1)$$

where g is the acceleration of gravity and Ω the angular velocity of the plate (in rad/sec, so $\Omega = 2\pi f$ with f the frequency). Depending upon these parameters, three cases have to be distinguished. First, if the rotation rate is fast enough, the fluid follows the potential rotation law $V(r) \sim 1/r$ and always rotates faster than the plate. In this case, which will be referred here as Dry-Potential (DP ; figure 1c), the results of TMBF remain unchanged. Reducing the rotation rate, keeping the potential model leads to the prediction of an inner zone in which the flow rotates faster than the plate. This unphysical feature, which was noted in a supplementary online material linked to TMBF, is corrected here by assuming that in this inner zone the flow rotates as a solid body with the angular velocity of the plate. Depending on the rotation rate, this inner region may be limited and still encircle a dry region (Dry-Composite or DC case ; figure 1b), or extend to the center and cover the whole plate, (Wet-Composite or W case ; figure 1a).

We will use ξ as the radius of the dry region (with $\xi = 0$ for case W), x as the radius of the solid-body rotation core (or more rigorously the radius where the velocity predicted by the potential law matches with that of the plate, which is outside of the flow in case DP), $\zeta = z(R)$ as the height of liquid at the wall of the container, and $z_0 = z(0)$ as the height at the center (for case W).

The angular velocity law is given by :

$$V(r) = \begin{cases} \Omega r & \text{for } \xi < r < x \\ \Gamma/(2\pi r) & \text{for } x < r < R. \end{cases} \quad (2)$$

The corresponding shape of the free surface can be deduced in a classical way from the computation of the pressure field, and is given in the three cases by :

$$\text{Case DP : } z(r) = \frac{1}{2g} \left(\frac{\Gamma}{2\pi R} \right)^2 \left(\frac{R^2}{\xi^2} - \frac{R^2}{r^2} \right). \quad (3)$$

$$\text{Case DC : } z(r) = \begin{cases} \frac{\Omega^2}{2g}(r^2 - \xi^2) & \text{for } \xi < r < x \\ \frac{\Omega^2}{2g}(x^2 - \xi^2) + \frac{1}{2g} \left(\frac{\Gamma}{2\pi} \right)^2 \left(\frac{1}{x^2} - \frac{1}{r^2} \right) & \text{for } x < r < R. \end{cases} \quad (4)$$

$$\text{Case W : } z(r) = \begin{cases} z_0 + \frac{\Omega^2}{2g}r^2 & \text{for } 0 < r < x \\ z_0 + \frac{\Omega^2}{2g}x^2 + \frac{1}{2g} \left(\frac{\Gamma}{2\pi} \right)^2 \left(\frac{1}{x^2} - \frac{1}{r^2} \right) & \text{for } x < r < R. \end{cases} \quad (5)$$

The model is thus characterized by three parameters, namely $[\Gamma, x, \xi]$ (or $[\Gamma, x, z_0]$ for case W) which have to be determined as function of the control parameter, which is the rotation rate of the plate Ω . Three equations are thus needed to solve. The first is provided by the continuity of the flow at $r = x$, namely:

$$\frac{\Gamma}{2\pi x} = \Omega x. \quad (6)$$

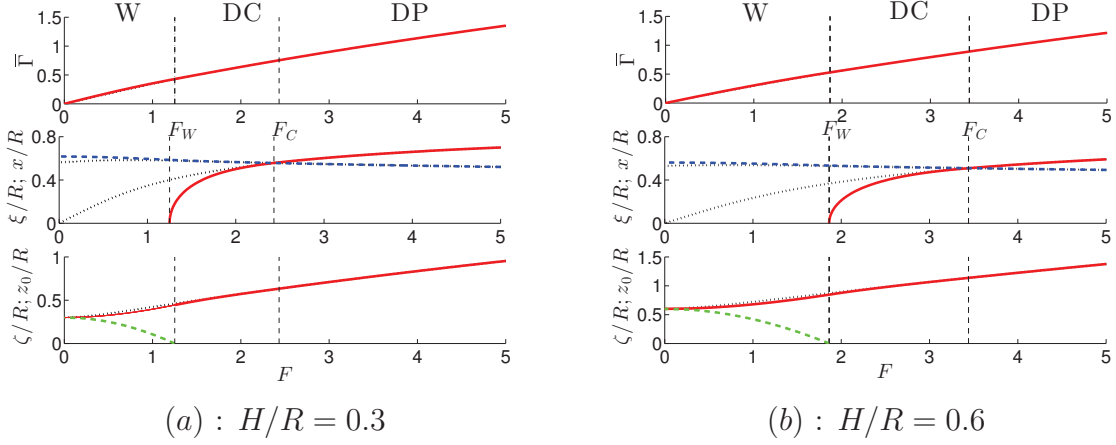


Figure 2. Characteristics of the composite model for (a) $H/R = 0.3$, and (b) $H/R = 0.6$, as function of the plate's Froude number. Upper plots : non dimensional circulation in the potential zone $\bar{\Gamma} = (\Gamma/2\pi\sqrt{gR^3})$; middle plots : ξ/R (plain, red) and x/R (dashed, blue) ; lower plots : ζ/R (plain, red) and z_0/R (green). The dashed vertical lines indicate the separation between the three regimes (W, DC and DP), and the thin dotted lines correspond, to the prediction of the previous model by Tophøj et al. (2013) which does not include a solid-body rotation zone.

The second one corresponds to the conservation of volume:

$$\int rz(r) 2\pi dr = \pi HR^2 \quad (7)$$

Finally, the third equation is taken as a balance of angular momentum, following the original idea of TMBF. This idea consists of equaling the accelerating torque due to the friction of the fluid with the plate (in the potential region) to the decelerating torque due to the friction with the wall. Assuming the boundary layers to be of turbulent type and modeling the skin friction as a quadratic drag leads to the following equation :

$$\int_{\max(x,\xi)}^R \left(\frac{r^2}{x^2} - 1 \right)^2 dr = \zeta, \quad (8)$$

where the lower bound of the integral is x in cases DC, W and ξ in case DP. Note that in cases DC and W, the inner zone (for $r < x$) gives no contribution to the skin friction since the flow and the plate rotate at the same angular velocity, thereby correcting a flaw of the TMBF model (see also supplementary online material of TMBF).

Figure 2 shows the characteristics of the model as function of F for two values of H/R , namely : the nondimensional circulation $\bar{\Gamma}$, the radius of the dry region ξ (for cases DC and DP), the radius of the solid-body rotation core x , the height of liquid at the outer bound $\zeta = z(R)$ and at the center $z_0 = z(0)$ (for case W). For high values of F , the Dry-Potential model of TMBF remains relevant. When the Froude number is decreased, a first transition occurs for a value $F = F_C$ where $x = \xi$ (see middle plots). Below this threshold, the Dry-Composite case is relevant, down to $F = F_W$ where $z_0 = 0$ (see lower plots) where the transition to the Wet-Composite case occurs. In all plots, the black dotted lines are the predictions from the original model of TMBF which is no

longer relevant in the W and DC cases. It is interesting to see that the circulation is almost the same in the original model ; on the other hand the radius ξ of the dry core substantially differs. Note that the radius of the solid-body rotation core x is almost constant, and in all cases in the range [0.5; 0.6].

2.2. The simplified "toy model"

In the sequel, we will investigate the stability of this flow through a simplified model. Following the original idea of TMBF, this "toy model" consists of restricting the flow to a narrow channel along the boundaries, as indicated by the dashed lines in figure 1. In the DP case (figure 1c), this "toy model" is identical as that of TMBF, and consists of two two-dimensional manifolds : a vertical cylindrical layer (segment BC) and a circular annulus (segment AC). In the two other cases, the latter region reduces to segment XC, and we add a third two-dimensional region, which is either an open annulus (case DC ; segment AX) or a full circle (case W ; segment OX).

3. Stability analysis

3.1. Flow expansion and matching conditions

For the stability analysis, we suppose that the flow is perturbed by a small perturbation of azimuthal wavenumber m and frequency ω . The positions of the upper free surface, the inner free surface, and the solid body rotation core are thus considered in the following way :

$$z = \zeta + \epsilon \zeta_1 e^{i(m\theta - \omega t)}, \quad (9)$$

$$r = \xi + \epsilon \xi_1 e^{i(m\theta - \omega t)}, \quad (10)$$

$$r = x + \epsilon x_1 e^{i(m\theta - \omega t)}, \quad (11)$$

with ϵ a small parameter. In the two vertical layers and the outer horizontal layer, the perturbation can be considered as potential, and is taken as follows :

$$\phi_c = \epsilon \left(K_1 (r/R)^m + K_2 (r/R)^{-m} \right) e^{i(m\theta - \omega t)} \quad (z = 0; r \in [x, R]) \quad (12)$$

$$\phi_g = \epsilon \left(K_3 e^{mz/R} + K_4 e^{-mz/R} \right) e^{i(m\theta - \omega t)} \quad (r = R; z \in [0, \zeta]) \quad (13)$$

In the inner, solid-body rotation layer, as the base flow is rotational, the perturbation cannot be assumed as potential. Instead, we work with the pressure, which is the solution of Laplace equation $\Delta p = 0$, and can be taken as :

$$p(r) = \epsilon \left(K_5 (r/R)^m + K_6 (r/R)^{-m} \right) e^{i(m\theta - \omega t)} \quad (z = 0; r \in [\xi, x]). \quad (14)$$

One should note that this approach, although not potential, is still inviscid. The velocity is defined as $\mathbf{u} = u_r(r) e^{i(m\theta - \omega t)} \mathbf{e}_r + u_\theta(r) e^{i(m\theta - \omega t)} \mathbf{e}_\theta$, and the components are deduced from :

$$u_r = \frac{i\epsilon}{\rho(\lambda^2 - 4)\Omega} \left[\frac{2mp}{r} - \lambda \frac{\partial p}{\partial r} \right], \quad (15)$$

$$u_\theta = \frac{\epsilon}{\rho(\lambda^2 - 4)\Omega} \left[\frac{\lambda m p}{r} - 2 \frac{\partial p}{\partial r} \right], \quad (16)$$

where λ is the non dimensional frequency in the rotating frame, defined as

$$\lambda = \frac{\omega - m\Omega}{\Omega}. \quad (17)$$

This derivation is standard, and can be found for instance in Ref. [9].

We now have to write down the equations which connects the layers. The condition at the corner C is the same as in TMBF, namely:

$$K_1 = K_3; K_2 = K_4. \quad (18)$$

At the free surface (point B), the kinematic and dynamic boundary conditions are (using the Bernoulli equation for the latter):

$$i(m\Omega_R - \omega)\zeta_1 = \partial\phi_g/\partial z; \quad i(m\Omega_R - \omega)\phi_g + g\zeta_1 = 0. \quad (19)$$

Eliminating ζ_1 , the two latter can be combined in a single equation :

$$(m\Omega_R - \omega)^2\phi_g = g\partial\phi_g/\partial z. \quad (20)$$

The matching at point X (for cases DC and W) leads to the following conditions :

$$\partial\phi_c/\partial r = u_r = i(m\Omega_R - \omega)x_1; \quad p = -i(m\Omega - \omega)\phi_c. \quad (21)$$

Finally, the free-surface conditions at point A (for case DC) lead to :

$$i(m\Omega_R - \omega)\xi_1 = u_r; \quad p + \left(\frac{\partial P}{\partial r} \right)_{r=\xi} \xi_1 = 0, \quad (22)$$

Where $P(r)$ is the pressure of the base flow, linked to the azimuthal velocity $V(r)$ given in Eq. (2) through the centrifugal balance $\partial P/\partial r = V^2/r$. The boundary conditions at point A can eventually be combined in a single one :

$$i(m\Omega - \omega)p + g_\xi u_r = 0; \quad \text{with } g_\xi = \left(\frac{\partial P}{\partial r} \right)_{r=\xi} = \xi\Omega^2. \quad (23)$$

Solving the stability problem now means finding the values of ω for which a nontrivial set of the coefficients $[K_1, K_2, K_3, K_4, K_5, K_6, \zeta_1, \xi_1, x_1]$ is possible. Technically, this requires writing the matching conditions in matrix form; the determinant of the matrix thus provides the *dispersion relation* $D(\omega) = 0$ whose roots are the possible frequencies (or *eigenvalues*). We will investigate separately the three possible cases depicted in figure 1, plus an additional interesting case.

3.2. Dry-Potential case

This case is the one treated by TMBF ; here the inner zone and the coefficients K_5, K_6 are not relevant, and the boundary condition at point A (Eq. 23) has to be replaced by

$$(\omega - m\Omega_\xi)^2 \phi_c(\xi) = -g_c \left. \frac{\partial \phi_c}{\partial r} \right|_{r=\xi}, \quad (24)$$

where $\Omega_\xi = \Omega(x/\xi)^2$, and $g_c = \xi\Omega_\xi^2$.

The dispersion relation can then be written in the following compact form :

$$D_{cp}(\omega)D_{gp}(\omega) = \frac{m^2 g g_c}{\xi R} (K^2 - 1), \quad (25)$$

with

$$K = \frac{1 + e^{-2m\zeta/R} \left(\frac{\xi}{R}\right)^{2m}}{1 - e^{-2m\zeta/R} \left(\frac{\xi}{R}\right)^{2m}}, \quad (26)$$

$$D_{cp}(\omega) = (\omega - m\Omega_\xi)^2 - g_c m K / \xi, \quad (27)$$

$$D_{gp}(\omega) = (\omega - m\Omega_R)^2 - gmK/R. \quad (28)$$

This dispersion relation is written in *wave interaction* form, as it takes the form of the product of two dispersion relations describing two types of waves, coupled by a small parameter. The dispersion relation D_{gp} is readily recognized as the dispersion relation for *gravity waves*. It has two branches of solutions $\omega = m\Omega_R \pm \sqrt{gmK/R}$, (noted waves G_+ and G_- in the following), which propagate in opposite way with respect to the frame of reference rotating with the flow at $r = R$. In the fixed frame, this means that the wave G_+ rotates faster than the flow while G_- is retrograde (i.e. rotates slower, or in the opposite direction). The dispersion relation D_{cp} was identified by TMBF as the one describing *centrifugal waves*, which are surface waves for which the role of the restoring force is played by centrifugal acceleration. The two solutions $\omega = m\Omega \pm \sqrt{g_c m K / R}$ (noted waves C_+ and C_-) rotate respectively faster and slower than the flow, but now at $r = \xi$.

TMBF investigated the possible resonances, which correspond to situations where two waves have the same frequencies. Following Cairns [8], such resonances lead to instability whenever the two interacting waves have energies of opposite sign; the wave energy (in the sense of Cairns) being defined as $\partial D / \partial \omega$. It can be verified that the wave energy is positive for branches G_+, C_+ and negative for branches G_-, C_- . Hence the criterion is met for the pair of waves (G_+, C_-) which effectively intersect. This wave interaction was proposed by TMBF to be at the origin of the rotating polygon instability.

3.3. Wet-Composite case

This case corresponds to $\xi = 0$. In this case, the matching conditions at the inner surface have to be replaced by the simpler condition $K_6 = 0$, which requires the solution to be bounded at $r = 0$.

The dispersion relation can be factorized into the following expression :

$$D_{gw}(\omega)D_{kw}(\omega) + \frac{2\Omega mg}{R}e^{-2m\zeta/R} \left(\frac{x}{R}\right)^{2m} = 0. \quad (29)$$

with

$$D_{gw}(\omega) = (\omega - m\Omega_R)^2 - mg/R, \quad (30)$$

$$D_{kw}(\omega) = \omega - \Omega (m - 1 - e^{-2m\zeta/R}(x/R)^{2m}). \quad (31)$$

Again this dispersion relation takes a *wave interaction* form. The first part $D_{gw}(\omega)$ still describes gravity waves (noted G_+ and G_-), while $D_{kw}(\omega)$ describes a single wave which is recognized as the *Kelvin-Kirchoff* waves (noted KK); namely the oscillation of a two-dimensional Rankine vortex. This can be recognized by noting that in the case where R and/or ζ is large, the frequency tends to the classical result $\omega \approx (m - 1)\Omega$ which is the oscillation frequency of a Rankine vortex in an infinite space (see [9] for instance). §

We can again investigate the possible resonances using the Cairns theory [8]. Here, the KK wave is found to rotate slower than the vortex core, and to have negative energy. Hence an unstable resonance involving waves G_+ and KK appears possible.

3.4. Dry-Composite case

This third case is a bit more complex, but the dispersion relation can still be written in wave-interaction form:

$$D(\omega) = D_{gd}(\omega)D_{kcd}(\omega) + e^{-2m\zeta/R} \left(\frac{x}{R}\right)^{2m} K_d(\omega) = 0 \quad (32)$$

with:

$$D_{gd}(\omega) = (\omega - m\Omega_R)^2 - gm/R, \quad (33)$$

$$D_{kcd}(\omega) = -\lambda^3 + (1 - a)\lambda^2 + (m + 2 - 2a)\lambda + m(1 - a), \quad (34)$$

$$K_d(\omega) = \begin{aligned} & [(\omega - m\Omega_R)^2 + gm/R] \\ & \times (-a\lambda^3 + (1 - a)\lambda^2 + (ma - 2a + 2)\lambda + m(a - 1)). \end{aligned} \quad (35)$$

(here $a = (\xi/x)^{2m}$).

Here, along with the gravity waves (G_+, G_-) described by $D_{gd}(\omega)$, the system displays new kinds of waves described by the relation $D_{kcd}(\omega)$. This relation has three roots which are always real, and noted KC_1 , KC_2 and KC_3 (in order of increasing frequency). The structure of these waves will be described further in section 4.3; as

§ Note that the oscillations of a Rankine vortex in a bounded space were also studied by Vatistas [10] who gave a dispersion relation with a slightly different form compared to (31), namely : $D_{kw'}(\omega) = \omega - \Omega (m - 1 + (x/R)^{2m})$. The differences are due to (a) the presence of the vertical layer which was not included in [10], and (b) to the fact that non-interacting problem leading to (31) actually corresponds to a zero-pressure boundary condition at the outer surface, instead of a non-penetration condition as in [10].

we will see they combine the characteristics of centrifugal and Kelvin-Kirchhoff waves, hence the designation. It is found that two of them (KC_1 , KC_2) are retrograde with respect to the vortex core and have negative energy, while the third one (KC_3) rotates faster than the vortex core and has positive energy. We hence anticipate the possibility of resonances involving G_+ and either KC_1 or KC_2 .

3.5. The solid-body rotation case

Before presenting the results, we briefly discuss the predictions of our stability approach in the case where the flow is in solid body rotation, with a dry core in the center. This situation is not encountered in our model, but it was proposed to be a relevant description of the flow in some previous studies [12, 13].

This case is obtained by setting $x = R$ in Eq. (32). This equation still describes the interaction between two gravity waves and three KC waves. However, in that case, since the angular velocities of the flow at the inner (point A) and outer (point B) surfaces are the same, all waves with positive energy (namely G_+ and KC_3) are located in the range $\omega > \Omega$, while all waves with negative energy (namely G_- , KC_1 and KC_2) are located in the range $\omega < \Omega$. Hence, it is impossible to have a crossing between two branches of opposite energies, which is the condition for instability according to Cairns theory [8]. We thus conclude that no instability is allowed by our model in that situation.

Note that a study of a solid-body rotation with inner surface was conducted by [13] who showed that this flow can stand large-amplitude deformations under the form of nonlinear waves. However, our present analysis shows that in the absence of any differential rotations, such patterns cannot spontaneously arise as the result of an instability.

4. Results

4.1. Phase diagram

Figure 3, which constitutes the main result of our study, depicts the range of existence of instabilities, for azimuthal wave numbers $m = 1$ to 5, as function of the two control parameters H/R and F . It is first notable that the present model predicts a range of instability for $m = 1$. This state is found to exist only in the "dry-composite" case, and for aspect ratios H/R comprised between 0.18 and 1.2. The range of instability for $m = 2$ consists of two parts. The first is contained in the Dry-Composite region and exists for $0.07 < H/R < 0.65$. The second one arises for $H/R > 1$ and splits into two branches; the lower rapidly enters the Wet region, while the upper one shifts upwards and eventually reaches the Dry-Potential region (for $H/R = 2$, outside of the range of the figure). For $m = 3$, the unstable region is a simply connected one; it starts from $H/R = 0.06$ in the Dry-Composite region, and splits in two branches for $H/R = 0.42$, the lower one entering the Wet region and the upper one moving towards the Dry-Potential region. The case $m = 4$ is again different. Here the unstable region consists of

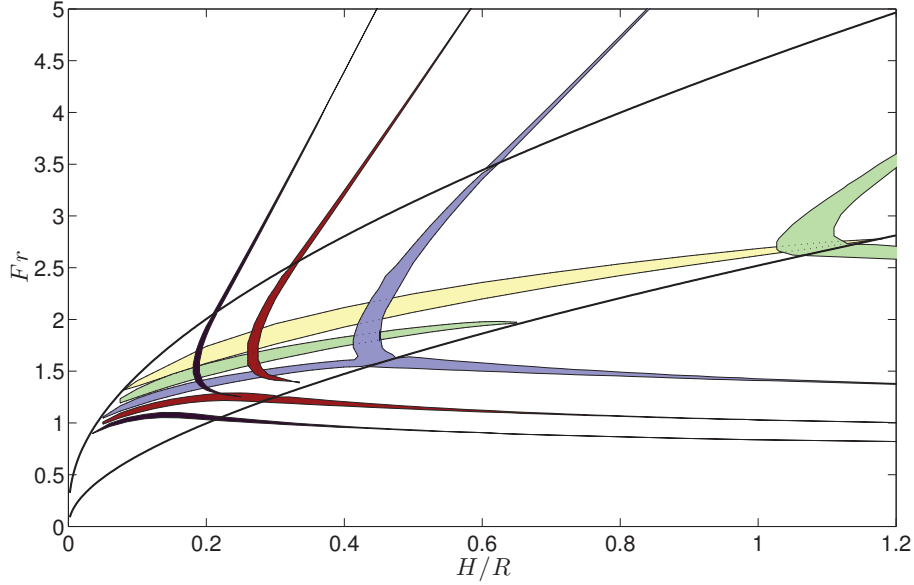


Figure 3. Parametric map of the unstable bands as function of H/R and $F = \Omega\sqrt{R/g}$. The colored areas correspond to the regions of instability for $m = 1$ (light yellow) to $m = 5$ (dark purple). The thick lines delimit the three regimes: Wet (lower region) ; Dry-Composite (middle region) ; Dry-Potential (upper region).

two parts. The first starts from $H/R = 0.06$ in the Dry-Composite region, and continues into the Wet region for $H/R > 0.29$. The second part arises for $H/R > 0.26$; it then splits into two branches, the lower one vanishing at the border of the Wet region for $H/R = 0.35$ and the upper one continuing into the Dry-Potential region for $H/R > 0.32$. The case $m = 5$ is qualitatively similar, and $m \geq 6$ also lead to the same picture.

Compared to the predictions of the simpler model of TMBF, this diagram of states is notably more complex. The latter study predicted that when increasing F , the instabilities are found with increasing values of m , starting from $m = 2$. This picture remains accurate in the upper part of the diagram corresponding to the "Dry-Potential" case. On the other hand, our study predicts that in the "Wet" case the instability bands occur in reversed order, i.e. the wavenumber (starting from $m = 2$) increases as the Froude number is decreased. The picture in the intermediate "Dry-Composite" region is even more complex, with in some cases three ranges of instability for the same wavenumber and the same value of H/R . Finally, another notable difference is the prediction of instabilities with $m = 1$, a situation which was not possible in TMBF. In practice, a perturbation with $m = 1$ corresponds to a 'monogon', or more properly to a precession of the dry core as a whole.

4.2. Study of branch interactions

To explain the complex features observed in figure 3, we will now investigate the solutions of the eigenvalue problem as function of F , for selected values of m and H/R (figures 4 and 5). In section 3.2, we have shown that the dynamics can be interpreted as an interaction between two families of waves. The first family is the gravity waves, which exist in the three regimes, and consist of two branches, noted G_+ and G_- . The second family differs according to the regimes ; in the Wet regime there is a single wave called KK ; in the Dry-Composite case there are three, noted KC_1 , KC_2 , KC_3 ; in the Dry-potential there are two, noted C_+ and C_- . We will show that the way these various branches reconnect is responsible for the qualitative differences observed between the various values of m in figure 3.

For $m = 1$, the branch KC_1 connects the KK and C_- branches, the branch KC_2 is disconnected, and the branch KC_3 connects to the C_+ branch. For $H/R = 0.3$ (figure 4a), the branch G_+ intersects the branch KC_2 , giving rise to instability in the center of the "Dry-Composite" area. As the Froude number is varied, the respective positions of these two branches are modified. For instance, for $H/R = 1.5$ (figure 4b), the lower termination point of the KC_2 branch passes above the G_+ branch. This explains why instability is no longer possible, and why the instability region in figure 3 ends up at the W/DP boundary. Similarly, for smaller H/R (not shown), the upper termination point of the KC_2 branch passes below the G_+ branch, explaining the vanishing of the unstable region at the DC/DP boundary. Note that in figure 4b an interaction also occurs along the G_- and KC_1 branches ; however here the Cairns criterion is not verified as both waves have negative energy. Accordingly, the resonance is stable and the branches avoid each other.

For $m = 2$, the branches are connected in the same way as for $m = 1$, and for $H/R = 0.5$ (figure 4c), the instability likely corresponds to interaction between G_+ and KC_2 branches. For $H/R > 0.65$, the KC_2 branch displaces upward and the branches no longer intersect (as for $m = 1$ in figure 4b), explaining the vanishing of the unstable region. However, when H/R is further increased, the branch KC_1 rises up and intersects twice with the G_+ branches, as illustrated by figure 4d for $H/R = 1.3$. This explains the recovery of instability and the subsequent splitting into two regions.

For $m = 3$, unlike the previous case, both KC_1 and KC_2 branches are connected with the KK branch at the W/DC boundary. For $H/R = 0.3$ (figure 5a), the instability corresponds to interaction between G_+ and KC_2 branches. For $H/R = 0.44$ (figure 5b), the G_+ branch interacts with both the KC_1 and KC_2 branches, explaining the widening of the unstable region observed in figure 3. When H/R is further increased, the unstable region splits in two parts, the first one entering the Wet region and involving the G_+ and KK branches, the second one involving G_+ and KC_1 (which latter becomes branch C_- when entering into the DP region).

For $m = 4$ (and higher values of m), the branches are connected differently at the W/DC boundary, as now the continuation of branch KK is branch KC_2 , while branch

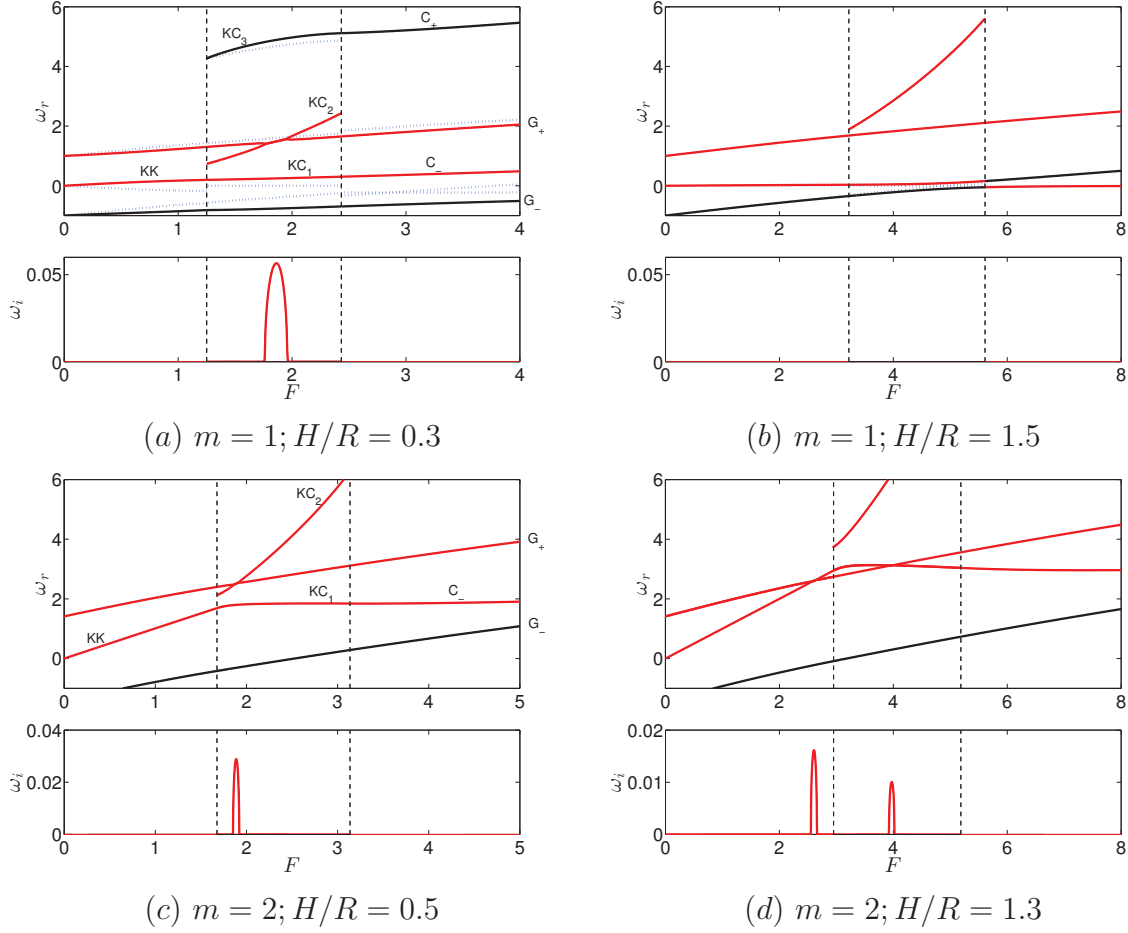


Figure 4. Eigenvalues (real and imaginary parts) for $m = 1$ and 2 , and selected values of H/R . The dashed vertical lines indicate the transitions between the three regimes (W / DC / DP). The branches along which an unstable interaction is possible (G_+ , C_- , KC_1 , KC_2 , KK) are indicated in red; the others in black (note that branches C_+ and KC_3 are outside of the range of the plots in most cases). The non-interacting branches (i.e. roots of the dispersion relations D_{gp} , D_{cp} , etc...) are in dotted lines ; note that the latter are hardly distinguished from the roots of the coupled system in most cases, except for $m = 1$. In the plots, ω_r and ω_i are nondimensionalized with $\sqrt{g/R}$.

KC_1 is disconnected. At low values of F , the instability first occurs as interaction between G_+ and KC_2 , and this branch smoothly continues as a G_+/KK interaction when entering into the Wet region. For $H/R = 0.28$ (figure 5c), the branch KC_1 moves upwards, and interacts twice with the G_+ branch, explaining the onset of the second instability region composed of two branches observed in figure 3. Increasing further the height to $H/R = 0.4$ (figure 5d), the upper branch continues into the DP region, as the KC_1 branch continues into the C_- one, but the lower branch vanishes at the DC/W boundary, as the KC_1 branch is disconnected.

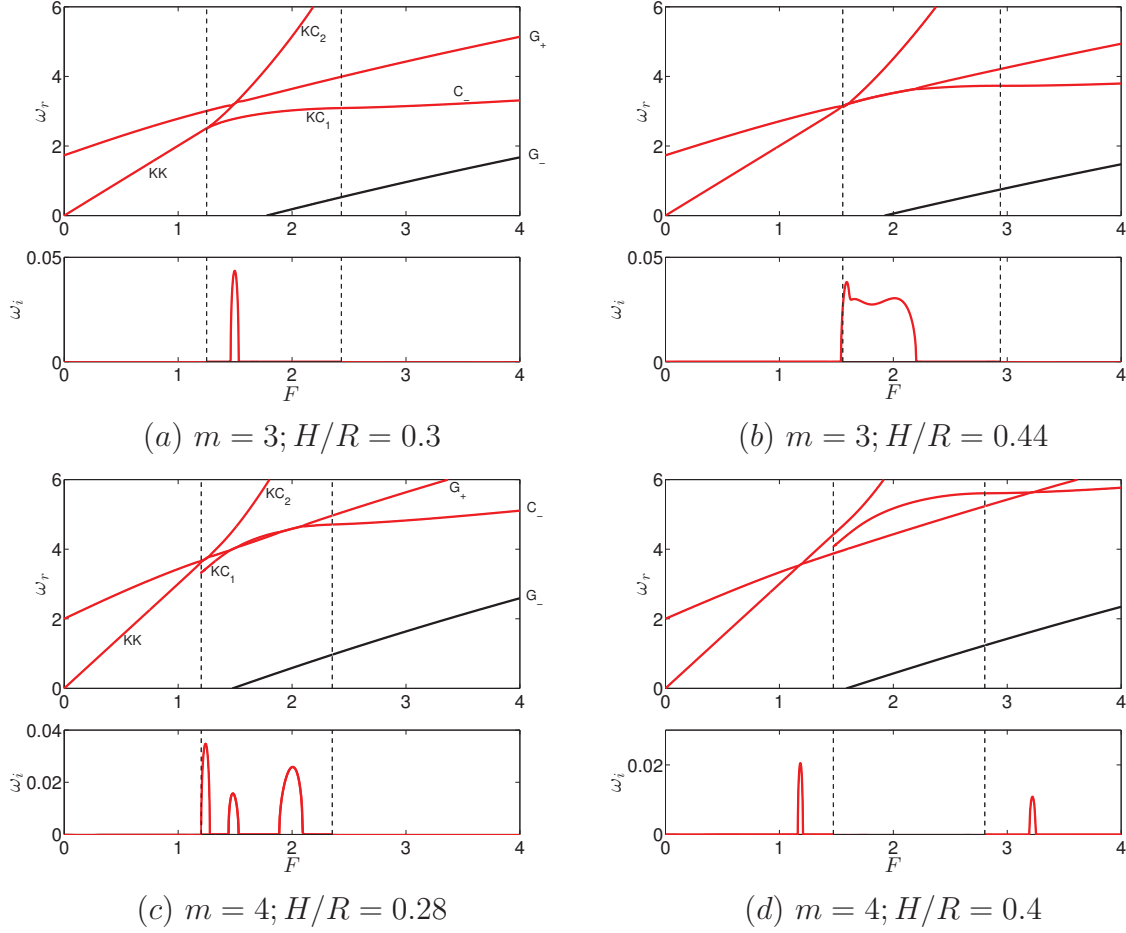


Figure 5. Eigenvalues (real and imaginary parts) for $m = 3$ and 4 , and selected values of H/R . Same legend as in figure 4.

4.3. Mode structure

Finally, we show in figure 6 a 3D reconstruction of the structure of some of the eigenmodes predicted by our model. The location of the upper and lower free surfaces are taken from Eqs. (9- 10- 11). The overall amplitude ϵ is arbitrary and chosen for visual convenience, but the ratio of amplitudes and phase shifts between the waves at the three surfaces are respected.

The three plots in the upper row illustrate the structure of the pure waves for a set of parameters located away from any resonance, namely ($m = 3, H/R = 0.25, F = 1.3$) (see figure 5(a)). It can be noted that for wave KC_1 (plot 6a) the deformation of the inner free surface and of the solid-body rotation core are in phase. The structure of the wave KC_3 (not shown) is very similar. This property indicates that these waves are mostly influenced by centrifugal effects at the inner surface, and that the solid-body rotation region mostly follows the dynamics imposed by the inner surface in a passive way. This interpretation is consistent with the fact that, at the DC-DP transition, the waves KC_1 and KC_2 always continuously reconnect with the centrifugal waves C_- and

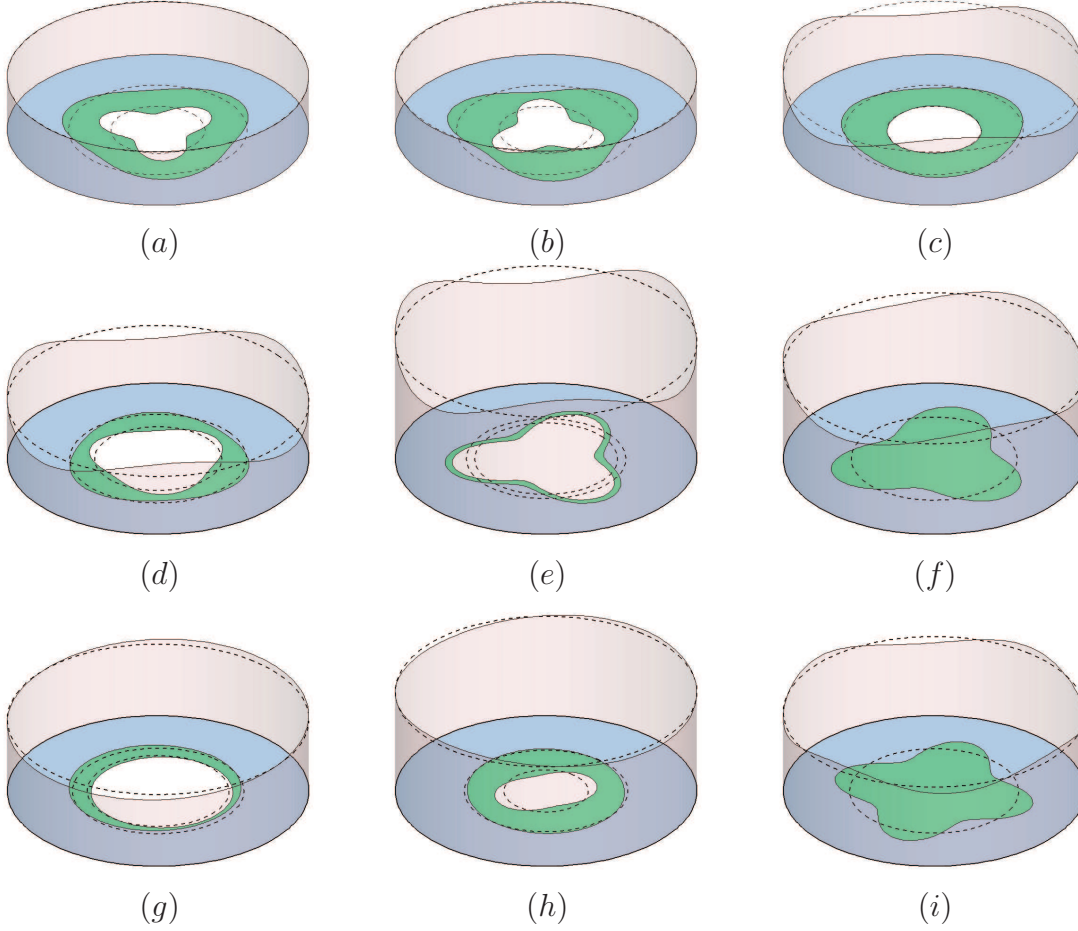


Figure 6. Illustration of the structure of some eigenmodes. The dashed circles indicate the mean position of each surface. The parameters for the cases displayed are as follows: (a) $m = 3$, $H/R = 0.25$, $F = 1.3$ (KC_1 wave). (b) $m = 3$, $H/R = 0.25$, $F = 1.3$ (KC_2 wave). (c) $m = 3$, $H/R = 0.25$, $F = 1.3$ (G_- wave). (d) $m = 3$, $H/R = 0.25$, $F = 1.5$. (e) $m = 3$, $H/R = 0.5$, $F = 1.57$. (f) $m = 3$, $H/R = 0.5$, $F = 2.64$. (g) $m = 1$, $H/R = 0.3$, $F = 1.85$. (h) $m = 2$, $H/R = 0.5$, $F = 1.9$. (i) $m = 4$, $H/R = 0.5$, $F = 1$.

C_+ . The structure of the KC_2 wave (plot 6b) is markedly different, as the deformation of the inner surface and core boundary are out of phase. This indicates that for this wave, centrifugal effects at the inner surface and vorticity dynamics within the solid-body region are both essential to explain the properties of this wave. Thus, this wave is really of an hybrid nature. This is consistent with the fact that this wave vanishes at the DC-DP transition. Plot 6(c) illustrates the structure of the wave G_+ for the same set of parameters ; this one hardly induces any motion at the inner surface.

The three plots in the middle row illustrate some unstable modes for $m = 3$. Plot 6(d) is for $H/R = 0.25$ where there is a single interval of instability for $m = 3$, corresponding to a resonance between KC_2 and G_+ branches (see figures 3 and 5a). The signature of the wave KC_2 is visible in this mode, the deformation of the inner free surface and of the solid-body rotation core being out of phase. Note that the deformation

of the upper surface has a $\pi/2$ phase shift with respect to the two latter. The two next plots are for $H/R = 0.5$ where the interval of instability splits into two bands (see figures 3 and 5b). Plot 6(e) corresponds to the unstable mode found in the upper band, and corresponds to resonance between G_+ and KC_1 waves. Plot 6(f) shows the mode found in the lower band, which belongs to the Wet regime. This one corresponds to an interaction between G_+ and KK waves.

Finally, the three plots in the lower row illustrate sample modes for other values of the azimuthal wavenumber. Plot 6(g) shows an example of an unstable mode for $m = 1$. The structure is a "monogon" characterized by out-of phase oscillations of the inner surface and solid-body rotation core, thereby indicating the presence of wave KC_2 (in accordance with figure 4(a)). Plot 6(h) shows an elliptical mode with $m = 2$, also caused by interaction of waves KC_2 and G_+ (see figure 4(c)). Finally, plot 6(i) displays a square ($m = 4$) wet mode, caused by interaction of waves KK and G_+ (see figure 5d).

5. Discussion

5.1. Effect of the azimuthal wavenumber

We have seen that in each of the three regimes (DP, DC, W), instabilities are found in narrow bands of the $[F, H/R]$ diagram, and that their occurrence can be explained as a resonance between waves belonging to different families and affecting different regions of the flow. However, the nature of the waves involved in the resonance and the dependence with the azimuthal wavenumber m of the range of instability is very different in each of the three regimes. In this section we summarize the properties of the unstable mode in each of the three regimes, and look for arguments to explain the dependency with respect to the azimuthal wavenumber m .

For strong rotations (Dry-Potential case), the instability is due to the interaction of a gravity wave affecting the upper free surface, and of a centrifugal wave, affecting the inner free surface. When increasing F , the instabilities are found with increasing values of m , starting from $m = 2$, a feature in good accordance with the order of apparition of the polygons in experiments. To explain this trend, we consider how the uncoupled waves behave when both F and m are assumed to be large. First, the gravity wave G_+ given by (28) can be approximated at leading order as $\omega_{G_+} = m\Omega_R + \sqrt{mgK/\bar{R}} \approx m\Omega_R$: the term involving gravity becomes negligible with respect to the term associated to rotation (in other words, the gravity wave becomes almost stationary in the frame rotating with the upper surface). On the other hand, the leading order approximation of the centrifugal wave is $\omega_{C_-} \approx (m - \sqrt{m})\Omega_\xi$. Equating both these leading orders leads to

$$\Omega_R/\Omega_\xi \approx \left(1 - \frac{1}{\sqrt{m}}\right).$$

So, for large m , the condition for resonance requires the ratio of rotation rates at both surface Ω_R/Ω_ξ to be very close to 1, and thus, as $\Omega_R/\Omega_\xi = (\xi/R)^2$, the inner surfaces ξ has to be very close to the cylinder wall R . Such conditions are only met for large

Froude numbers, when the flow is strongly pushed against the vertical wall by centrifugal effects.

For weak rotations (Wet case), the mechanism is different, and now involves the interaction of a Kelvin-Kirchhoff wave corresponding to a deformation of the boundary of the vortex core with the gravity wave. Interestingly, the bands of instability in this regime occur in reversed order, and their location is almost independent of the value of H/R . This can also be understood by looking at the behavior of the frequencies of the uncoupled waves for large m . Here, the leading order of the gravity wave is $\omega_{G+} = m\Omega_R + \sqrt{mgK/R} \approx m\Omega_R + \Omega\sqrt{m}/F$, and the leading order of the KK wave is $\omega_{KK} = (m-1)\Omega$. Equating the two leading orders lead to

$$F \approx \frac{1}{[1 - (\Omega_R/\Omega)]\sqrt{m}}.$$

Now, according to figure 2, the ratio $\Omega_R/\Omega = (x/R)^2$ is almost independent of H/R and F in all the wet regime, with value $\Omega_R/\Omega \approx (0.6)^2$. The formula given above thus explains both the inverse dependency with m of the Froude corresponding to resonance, and the almost independence with respect to H/R .

The situation in the Dry-Composite case is, at first glance to figure 3, far more complex. However, there are actually only two kinds of resonances. The first type is found along the instability bands which enter the Dry-Composite range from above, as a continuation of the unstable bands existing in the Dry-Potential range. These instabilities involve the KC_1 waves, whose structure, characterized by in-phase motion of the inner surface and the vortex boundary, is actually very close to that of the centrifugal waves (see e.g. figure 6e).

The second type of instabilities in the Dry-Composite case involve the KC_2 waves. The latter are always characterized by substantial deformation of the vortex core (see e.g. figure 6a), and are thus more related to the KK waves existing in the Wet regime. The general organization of the unstable bands is also more akin to that in the Wet regime, with almost horizontal bands occurring in reverse ordering. However, the connection between KC_2 and KK waves only exists for $m \geq 3$. The cases $m = 2$ and $m = 1$ are thus a bit particular, with a vanishing of the band corresponding to this type of instability at the DC/W connection.

5.2. Comparison with experiments

We now discuss the relevance of our theoretical predictions with respects to available experimental results.

The relevance of the interaction between gravity and centrifugal waves to explain the polygonal patterns was already demonstrated in TMBF. The present study shows that, although this interaction only occurs in its purest form in the Dry-Potential case, it is still relevant in the upper half of the Dry-Composite range of the state diagram, where there exist a type of composite waves (KC_1 waves) which are qualitatively similar to the centrifugal waves existing in the purely potential cases. This points gives us

further confidence in the arguments of TMBF, by showing that the gravity/centrifugal interaction mechanism is still accurate if the base flow presents an inner solid-body rotation of limited extent.

A second striking prediction of our model is the existence of a new mechanism, involving gravity and Kelvin-Kirchhoff waves, existing in its purest form in the Wet regime. We propose this mechanism to be at the origin of the sloshing phenomenon observed in experiments in the same range of parameters. The range of existence of the sloshing phenomenon was particularly described in the experiments of Iga et al.[5]. In particular, the range of existence of the sloshing behavior with azimuthal wavenumber $m = 3$ in figure 5 of [5] is strikingly similar to the range of existence of the $m = 3$ 'Wet instability' in our theoretical diagram (figure 3). In both cases, the range is a very narrow band with nearly constant Froude number ($F \approx 1.8$ in the experiment ; $F \approx 1.4$ in our model). The bands also occur in the same range of aspect ratios, namely $H/R \in [.4, .9]$. The range of existence of sloshing with $m = 2$ is also well predicted by our model, namely $F \approx 3$ and $H/R = 1$ while [1] observed this state for $F \approx 2.8$ and $H/R \approx 0.84$, and [5] for $F \approx 3$ and $H/R \approx 0.9$. Additional experiments should be conducted to confirm our interpretation of the sloshing mechanism. First, our analysis predicts instability in the wet regime for azimuthal wave numbers $m \geq 2$, while only sloshing with $m = 2$ and $m = 3$ was observed. One should thus check if sloshing with $m \geq 4$ also occurs at lower values of F . Secondly, our interpretation involves the existence of a Kelvin-Kirchoff wave propagating along the boundary of the vortex core. This point should also be confirmed by detailed velocity measurements, as such a motion is not directly visible at the free surface.

The predictions of our model in the intermediate, Dry-Composite case are more puzzling. First, the situation for $m = 2$ is peculiar: the model predicts that perturbations with this wavenumber are stable in the range $H/R \in [0.7, 1]$, and that below this range $H/R < 0.7$ instabilities with $m = 2$ appear at higher Froude number than the ones with $m = 3$. This is not consistent with experiments, where elliptical patterns have the largest range of existence and always occur at lower Froude numbers than the polygons with $m \geq 3$. The prediction of instability with $m = 1$ is also puzzling, as such a behavior was not observed in experiments with a rotating bottom. However, one should point out that a "monogon" pattern was actually observed by [11] in a slightly different experimental setup in which both the bottom plate and the outer vertical wall are put into rotation in a differential way.

5.3. Perspectives

In this work, we have studied the stability properties of the swirling flow in a cylindrical tank with rotating bottom through a very simplified approach, which reduces the flow to its very essential aspects by assuming that the whole motion occurs within a narrow channel along the walls. Despite its extreme simplicity, this approach is able to predict the onset of three-dimensional patterns at both large rotation rates (Dry-Potential case)

and weak rotation rates (Wet case), to interpret them as wave-interaction phenomena, and to explain their range of existence in a qualitative way.

In order to make these predictions more quantitative and to clarify the situation in the range of intermediate rotation rates (corresponding to the Dry-Composite range of the present model), we are now continuing this study using a global stability approach, which fully retains the spatial structure of the base flow and of the perturbations. Preliminary results were given in TMBF (for the potential flow) and in Ref. [12] for both the solid-body rotation case and the composite case. This approach allows for a much larger diversity of waves (and hence of possible interactions). First, each family of waves is actually composed of an infinite set, each described by a radial wave number, instead of the 2 or 3 leading ones captured by the present model. These waves are not described by the simple model explained in detail in the present paper but preliminary results [12] show that some of them can resonate. Secondly, when a zone in solid body rotation is retained, the global approach captures two entirely new families of waves: first the 'topographic' Rossby waves associated to the radial variation of the liquid height and secondly the inertial waves due to the Coriolis acceleration. Future efforts should also improve the modeling of the base flow, beyond the simple potential and composite cases considered so far. In particular, the boundary layers as well as the secondary flow should be incorporated into the base flow modeling.

Finally, the linear stability approach employed here can not explain some important features associated with large-amplitude patterns. In particular the hysteresis phenomenon associated to the transition between axisymmetric flow and elliptic pattern [4, 5], the recurrent behavior displayed by both the "switching" and "sloshing" phenomena, and eventually the large zone of existence of the polygons compared to the stripes of instability seem to be due to non linear effects. A theoretical study using a weakly nonlinear approach is underway, and the preliminary results are promising.

Acknowledgements

We would like to acknowledge Tomas Bohr, Erik Linnartz, and Keita Iga for stimulating discussions and for the generous sharing of unpublished results. The French Direction Générale de l'Armement (DGA) is acknowledged for funding the PhD of J. M. Finally, D.F. is grateful to Flavio Giannetti and Paolo Luchini for providing the numerous Pizze & Gellatti involved in the completion of this paper, during a pleasant stay at Università di Salerno.

- [1] G. H. Vatistas, *J. Fluid Mech.* **217**, 241–248 (1990).
- [2] T. R. N. Jansson, M. P. Haspang, K. H. Jensen, P. Hersen and T. Bohr, *Phys. Rev. Lett.* **96**, 174502 (2006).
- [3] T. Suzuki, M. Iima and Y. Hayase, *Phys. Fluids* **18**, 101701 (2006).
- [4] Y. Tasaka and M. Iima, *J. Fluid Mech.* **636**, 475–484 (2009).
- [5] Keita Iga, Sho Yokota, Shunichi Watanabe, Takashi Ikeda, Hiroshi Niino and Nobuhiko Misawa, "Various phenomena on a water vortex in a cylindrical tank over a rotating bottom", Submitted to *Fluid Dyn. Res.*

- [6] L. Tophøj, J. Mougel, T. Bohr and D. Fabre, *Phys. Rev. Lett.* **110**, 194502 (2013), In the text it is referred to as TMBF.
- [7] R. Bergmann, L. Tophøj, T. A. M. Homan, P. Hersen, A. Andersen and T. Bohr, *J. Fluid Mech.* **679**, 415–431 (2011) and Erratum **691**, 605 (2012).
- [8] R. A. Cairns, *J. Fluid Mech.* **92**, 1–14 (1979).
- [9] P. G. Saffman, *Vortex Dynamics*.
- [10] G. H. Vatistas, J. Wan and S. Lin, *Acta Mechanica* **103**, 89–102 (1994).
- [11] B. Bach, E. C. Linnartz, M. H. Vested, A. Andersen and T. Bohr, submitted to *J. Fluid Mech.*
- [12] J. Mougel, D. Fabre, L. Lacaze, Accepted for publication in *Mechanics & Industry*.
- [13] M. Amaouche, H. A. Abderrahmane, G. H. Vatistas, *European J. Mech.* **41**, 133–137 (2013).